npj Heritage Science

https://doi.org/10.1038/s40494-026-02519-2

Article in Press

Hidden evolving anisotropic order in Pollock's drip paintings

Received: 14 January 2026

Accepted: 31 March 2026

Cite this article as: Pedretti, D. Hidden evolving anisotropic order in Pollock's drip paintings. *npj Herit. Sci.* (2026). https://doi.org/10.1038/s40494-026-02519-2

Daniele Pedretti

Hidden evolving anisotropic order in Pollock's drip paintings

Daniele Pedretti*

Dipartimento di Scienze della Terra "A. Desio", Università degli Studi di Milano (UNIMI), 20133, Milan, Italy

*Corr. Author email: daniele.pedretti@unimi.it

Abstract

Jackson Pollock's action paintings (1943–1954) combined rapid drip-and-pour gestures with large-scale Lévy-flight movements, producing complex, apparently chaotic patterns. Here, directional geological entropy (DGE), a Shannon-entropy–based framework originally developed for heterogeneous geological systems, is applied to 47 digital images of Pollock's works. The analysis reveals a previously unreported and systematic anisotropy in spatial order, with consistently higher disorder along the horizontal direction than along the vertical one. This directional asymmetry evolves over time, being strongest in early works (1943–1947) and progressively decreasing as Pollock's technique matures. DGE also captures a transition from comparatively ordered to highly disordered patterns, followed by a regime of stable, near-maximum entropy. These findings establish DGE as a powerful alternative to fractal analysis and demonstrate its ability to uncover directional structure in complex visual patterns, extending entropy-based methods to the quantitative study of artistic heritage.

Introduction

In visual and musical arts, patterns such as painted traces or sound sequences are often perceived as chaotic and unstructured, yet their complexity can frequently be described using mathematical and statistical models. The work of abstract expressionist Paul Jackson Pollock (1912–1956) provides a well-studied example. His drip-and-pour paintings, created during the "action painting" period beginning in 1943 and extending until 1954 have long attracted the attention of scholars seeking to explain their complexity through statistical physically based models.

The most influential quantitative approach has been the fractal analysis pioneered by Taylor *et al.* [1,2]. Applying box-counting to high-resolution digital images, they identified fractal scaling in Pollock's works and distinguished two characteristic fractal dimensions (D): a short-scale (centimeter-scale) D associated with paint drips and a long-scale (meter-scale) D linked to Pollock's bodily movements across the canvas. During the action-painting years, Pollock's fractal dimension expanded from roughly $D=10^{-1}$ m² to $D>10^{1}$ m². Subsequent studies have examined these fractal-like structures in increasing detail [3–6], proposing that fractals arise naturally from Pollock's combination of short-scale drip-and-pouring and long-scale Lévy-flight motions. Fractals thus provide evidence that Pollock's apparently chaotic images embody underlying structure[7,8]. Fractals have even been suggested as tools for Pollock's paintings authentication [9].

However, Pollock did not intentionally paint fractals. Although his energetic process was a deliberate and calculated effort to express internal states, as famously documented by Hans Namuth in 1950[10], it is unlikely that Pollock followed any fractal model. Several researchers have critiqued aspects of the fractal interpretation[11,12], arguing, for example, that the limited size

of Pollock's canvases prevent true self-similarity across the many orders of magnitude required for robust power-law scaling. Thus, while fractal theory remains a strong, physically grounded explanation for some aspects of Pollock's patterns, alternative statistical approaches may also offer valuable insights into his revolutionary painting method. Nevertheless, applications of non-fractal statistical models to Pollock's work remain limited[13–16].

Shannon's information entropy[17] is a powerful framework for assessing pattern complexity. Although fractal dimensions are related to spatial entropy[18,19], the two differ fundamentally. Entropy quantifies disorder or information loss and varies with measurement scale, whereas fractal dimension is scale-independent[20]. Machado and Lopes [13] used Shannon entropy to analyze 11 Pollock paintings as part of a broader survey of artworks from the last seven centuries, and Pessa and Ribeiro [16] applied permutation entropy to *Number 1, 1950 (Lavender Mist)*. To our knowledge, however, no study has examined Pollock's action paintings through the lens of scale-dependent information entropy or related it to the temporal evolution of his artistic practice.

Here, 47 Pollock paintings from 1943–1954 were analyzed using the geological entropy framework[21,22]. Based on scale-dependent Shannon entropy, geological entropy quantifies spatial order or disorder in complex patterns across varying observation scales[21,22]. Originally developed to characterize geological features such as alluvial aquifers, which exhibit complex, seemingly chaotic, fractal-like structures[23–25], geological entropy has been applied to heterogeneous hydraulic conductivity fields, porosity distributions, and fracture networks[21,26–28]. The tool GEOENT[29] was developed to for calculating directional geological entropy (DGE) and deriving anisotropic geological entropy metrics along Cartesian directions.

This study pursues three main objectives. First, we test the hypothesis that Pollock's paintings, long described as fractal-like, can be effectively analyzed also using geological entropy, which was designed to quantify spatial order in complex patterns in fixed-length systems, like Pollock's canvas. Second, we investigate whether DGE can reveal aspects of Pollock's work not captured in previous analyses, particularly the presence and evolution of anisotropy in spatial order, an underexplored feature when analyzing Pollock's Action Painting works[30]. Third, we assess the broader applicability of geological entropy beyond geosciences, using Pollock's paintings as a test case for analyzing non-geological patterns, and the comparison against fractal analysis for validation.

Methods

Directional geological entropy

Geological entropy is based on Shannon's information entropy (H), which evaluates the marginal probabilities of occurrence of a discrete variable (i.e., a category) within a finite subdomain. Higher H values indicate greater spatial disorder, meaning that all categories have similar marginal probabilities within the subdomain. Conversely, lower H values indicate the presence of a predominant category, suggesting higher spatial order.

Using directional geological entropy (DGE), the entropy H is computed over increasing spatial scales and along different directions. The procedure begins with an initial isotropic block of values, which is progressively expanded until it reaches a specified size, constrained by the dimensions of the dataset. This process produces an entrogram, which is a graph that shows how H changes as block size increases and serves a role analogous to the variogram used in

geostatistical analysis. In this study, DGE is applied to a two-dimensional system suitable for the analysis of digital images such as those of Pollock's paintings, although the method was originally developed for use in three-dimensional systems.

A first metric to be defined is the relative entropy (H_R), which can be computed as

$$H_R(\boldsymbol{l}) = \frac{\sum_{i=1}^{n_b} p_{L,i}(\boldsymbol{l}, n_b)[\ln p_{L,i}(\boldsymbol{l}, n_b)]}{H_0} \quad (1)$$

where $\boldsymbol{l} = l_x\,\hat{\boldsymbol{\imath}} + l_y\,\hat{\boldsymbol{\jmath}}$; $\hat{\boldsymbol{\imath}}, \hat{\boldsymbol{\jmath}}$ are the unit vectors parallel to the Cartesian directions *x* and *y* respectively ($i.e., \hat{\boldsymbol{\imath}}$ = (1, 0); $\hat{\boldsymbol{\jmath}}$ =(1 ,0)); l_x, l_y are the scalar components of $\boldsymbol{l}$, which also correspond to the entrogram lag or bandwidth (bw); n_b is the number of categories for a discrete random variable or the total number of bins used to discretise the probability density function of a continuous variable; $p_{L,i}(\boldsymbol{l})$ is the local proportion, or marginal probabilities, of occurrence of the categories within the subdomain; H_0 defines the entropy calculated for the entire system. Equation (1) can be computed at any location of the grid (*i.e.,* any image pixel). To obtain a single representative value of $H_R(\boldsymbol{l})$ for the analysed image, in GEOENT a number of locations are randomly selected within the domain using a quasi-random discrepancy sequence (Sobol LPτ). Keeping the same subdomain size, an average relative entropy is then computed and used for the image analysis.

A special case of (1) is when searching box is at its smallest scale, *i.e.*, a square of size $l_x = l_y = 1$ unit, where the unit is the grid size of the input dataset (*i.e.*, a picture pixel in this work). We define this amount as the short-scale, or one-lag, relative entropy

$$H_{R0} = H_R(l_x, l_y = 1) \quad (2)$$

The normalization in Equation 1 is such that $H_{R0} = [0,1]$. More ordered systems tended to lower H_{R0} , while more disordered systems are characterized by $H_{R0} \rightarrow 1$[21].

The calculation of the relative geological entropy can be repeated for larger subdomains. When $H_R(\boldsymbol{l})$ *is* plotted against the increasing lags, it forms the entrogram curve. The searching box can grow identically in each direction ($l_x = l_y$) to obtain 'isotropic' entrograms. The extension of the searching box is also called bandwidth (bw). If one direction grows more than other, the searching box is rectangular, resulting in an anisotropic, or directional entrogram, defining the concept of directional geological entropy (DGE). For a direction i, an entropic scale (Hs) can be calculated to quantify the spatial order of a random field, as

$$Hs_i = \int_0^{\infty} [1 - H_R(l_i)]\mathrm{d}l \tag{3}$$

In the case of non-rectangular 2D domains, the searching box can grow more in one direction than in the others. Therefore, it is useful to normalise Hs by the size of the searching box in a specific direction. A normalised entropic scale, nHs, is thus calculated such that

$$nHs_i = \frac{nHs_i}{\max(l_i)} \tag{4}$$

where $\max(l_i)$ is the maximum bandwidth of the searching box along the i^{th} direction. Along one direction, an image showing larger nH_s and presents higher persistency of patterns of spatial association of certain categories and, therefore, spatial order in their spatial structure. In other words, the more ordered a variable is along a specific direction, the longer a directional entrogram will take to reach the asymptotic value[22]. In this sense, nH_s is inversely correlated with H_{R0} for what concern measuring the order of a random pattern.

Since geological entropy is computed on bidimensional images, in this work $i = x$ or y, where x denotes the horizontal direction and y the vertical direction. An anisotropy ratio ε was then calculated as

$$\varepsilon = \frac{nHs_x}{nHs_y} \tag{5}$$

To illustrate the conceptual meaning of directional geological entropy, Figure 1 presents the entrograms and associated metrics for two idealized images. The image on the left (Figure 1a) shows a square, or checkerboard, pattern, whereas the image on the right (Figure 1b) displays a striped pattern. Stripe patterns are more persistent along the horizontal direction x. They require periodic organization in only one direction, while square or checkerboard patterns require simultaneous ordering in two independent directions. Because it is generally easier for a system to align in a single direction than in two, stripe patterns are more common and more stable and therefore appear more ordered. From the perspective of information entropy, each pattern type, whether striped or square, can be regarded as a “macrostate" that provides a coarse description of the system. Each macrostate corresponds to many possible “microstates”, defined by the exact pixel or particle configurations. A larger number of microstates implies higher entropy, whereas fewer microstates imply lower entropy and thus greater order.

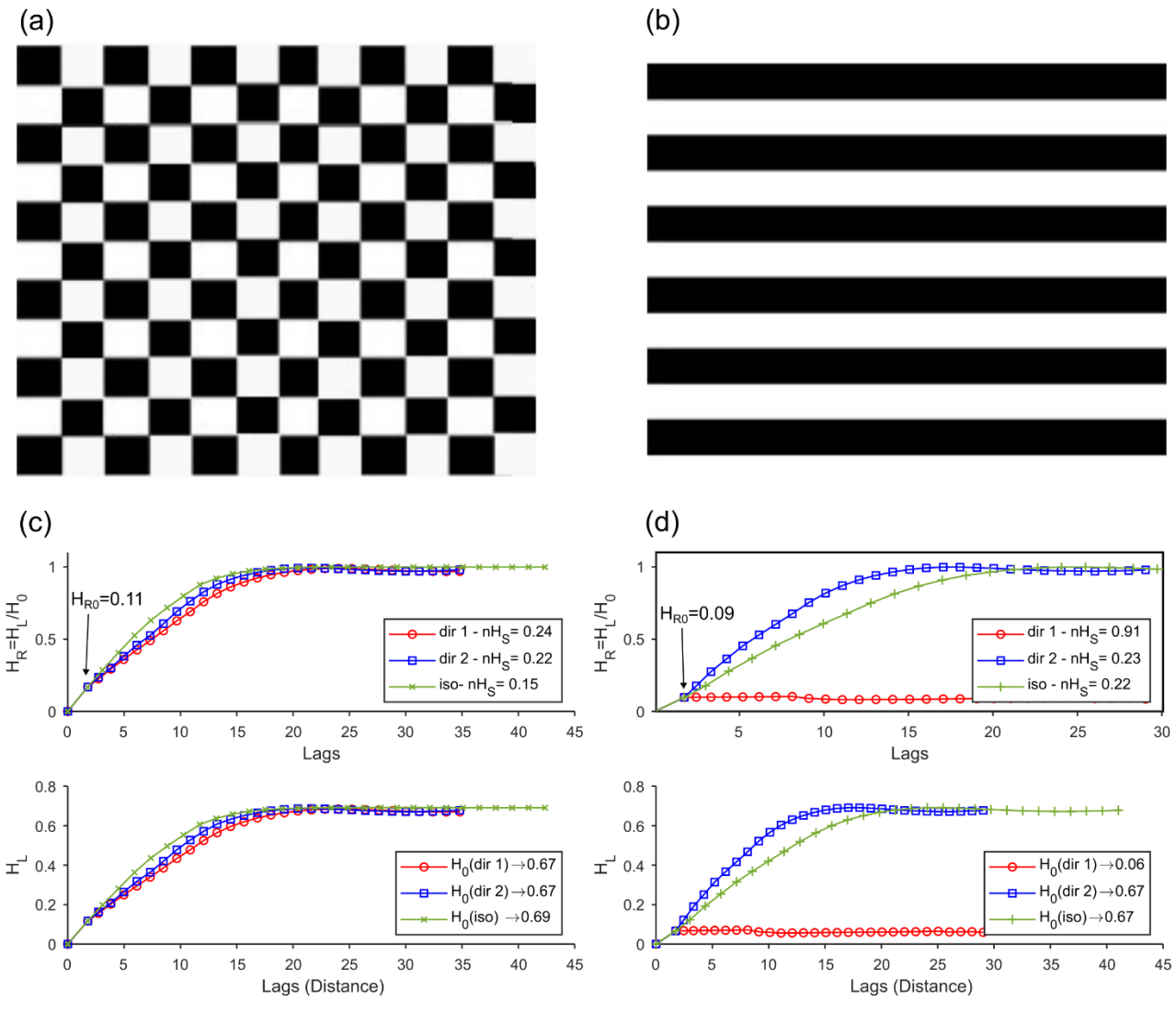

The entrograms of the square patterns (Figure 1c) show an isotropic increase in relative entropy that approaches values close to the maximum entropy of the system, which for a binary case is $H_{\max} = 0.67$. In contrast, the striped pattern exhibits greater persistence along the horizontal direction, corresponding to a much larger entropic scale. In addition, the relative entropy at one lag (H_{R0}) is lower for the more ordered striped pattern than for the more disordered square pattern.

Analyzed Pollock's images

The DGE indicators (H_{R0}, H_0, nHs_i) were calculated using the code GEOENT[29] on digital images (photographic pictures) representing Pollock's paintings between 1943 and 1954, i.e., the period generally associated to the Action Painting period by the artist and comprising also the last years of the artist' life.

The images were found on the web through a traditional search engine and screen-captured or downloaded locally (not distributed to avoid potential copyright issues). Images were saved at their maximum possible resolution as compressed JPG files. If more files for the same pictures were found, those with the highest resolution were kept. Since Pollock's paintings were created in different years and have different sizes, we analyzed only those images for which information related to the canvas sizes and specific creation years were available.

In total, 47 images were analyzed. Table 1 lists the painting name, year of creation, image resolution (in pixels) and canvas sizes (in cm) corresponding to the analyzed images. While the Action Painting period is generally considered to begin in 1943 with *Composition with Pouring II*, relatively few earlier works fall within this stylistic category. Consequently, the number of early paintings is inherently limited. Despite this constraint, the analyzed dataset size remains comparable to, or larger than, those used in several well-cited fractal analyses of Pollock's work[30,31], supporting the robustness of the analysis.

Note that these images had very different resolutions. This implies that, for the same canvas size, smaller-scale features can be revealed from the analysis of higher resolution images. Using GEOENT, entrograms are designed to deal with the different image resolutions, as the lag scale

in each direction (dl) and the maximum bandwidth size in each direction, $\max(l_i)$, are normalized by the pixel size, computed as

$$\mathrm{dx} = \mathrm{N_x}/\mathrm{L}_X \quad \mathrm{dy} = \mathrm{N_y}/\mathrm{L}_y \qquad (6)$$

where N_x and N_y represent the number of pixels along the horizontal and vertical image direction, respectively, and L_X and L_y are the canvas size along the horizontal and vertical directions, respectively. The computation of directional indicators using GEOENT can be demanding for large bandwidth sizes (bw>100). Therefore, after an initial sensitivity analysis around bw reported in the *Supplementary Information* (Figures S1-S6*),* for a specific direction *i*, a bandwidth size bw_i=50 and bw_j=1 (where *j* is the direction orthogonal to *i*) was considered a sufficiently accurate trade-off, as statistical-equivalent results were to those obtained using a larger bw but with reduced computational time. In the isotropic case, the bandwidth size was bw_i= bw_j=50.

Image resolution may, however, affect H_{R0}, which is computed at the first lag, corresponding to one image pixel. Hence, H_{R0} could be sensitive to resolution. To assess whether resolution significantly influences H_{R0}, we conducted a sensitivity analysis by filtering the images using different resolution thresholds ($thre$), up to $thre$=1000 pixels in the horizontal direction. The results, presented in the *Supplementary Information* (Figures S7-S10) indicate that thresholds from *thre*=0 to *thre*=500 pixels yield qualitatively similar conclusions to those obtained using the full dataset. When the threshold is increased to *thre*=1000 pixels, the results change. However, the number of available images is substantially reduced to only 10, which is insufficient to support a robust statistical analysis of temporal trends. Accordingly, no resolution thresholds were applied in the main analysis, and geological entropy metrics were computed using the entire dataset.

Table 1 Name of the analyzed Pollock's paintings, their original canvas size, the resolution of the JPG file used in this study and the corresponding pixel size, for the vertical (y) and horizontal (x) directions.

Painting name	Year	Canvas size (cm)		JPG file resolution		Pixel size (cm)	
		L_Y	L_X	N_Y	N_X	dy	dx
Mural	1943	243	604	637	1596	2.62	2.64
Composition with Pouring II	1943	64	56	793	696	12.39	12.43
Eyes in the heat	1946	137	109	783	613	5.72	5.62
Free Form	1946	49	35	598	424	12.20	12.11
Shimmering Substance	1946	76	62	3070	2457	40.39	39.63
Lucifer	1947	104	267	696	1747	6.69	6.54
Galaxy	1947	110	86	797	615	7.25	7.15
Reflection of the Big Dipper	1947	111	92	492	407	4.43	4.42
Alchemy	1947	114	195	295	567	2.59	2.91
Watery paths	1947	114	86	4083	3108	35.82	36.14
Sea change	1947	147	112	3984	2996	27.10	26.75
Enchanted forest	1947	221	115	571	301	2.58	2.62
Paradigm C2	1948	122	254	2506	5176	20.54	20.38
Number 1	1948	173	264	750	1152	4.34	4.36
Number 3	1948	77	57	596	436	7.74	7.65
Number 5	1948	240	120	772	459	3.22	3.83
Number 6	1949	112	137	389	472	3.47	3.45
Summertime: Number 9A	1948	85	555	210	1413	2.47	2.55
Number 13A (Arabesque)	1948	94	297	1216	3840	12.94	12.93
Number 19	1948	78	57	799	581	10.24	10.19
Number 20	1948	52	66	3720	4688	71.54	71.03
Number 23	1948	58	78	519	722	8.95	9.26
Silver Over Black, White, …	1948	61	80	581	900	9.52	11.25
Number 1	1949	160	260	1991	3220	12.44	12.38
Number 3	1949	156	95	796	475	5.10	5.00
Number 7 (Out of the Web)	1949	122	244	643	1274	5.27	5.22
Number 8	1949	86	182	501	1055	5.83	5.80
Number 10	1949	46	272	152	945	3.30	3.47
Number 12	1949	79	57	564	399	7.14	7.00

Number 17	1949	57	72	437	566	7.67	7.86
Number 32	1949	79	57	798	588	10.10	10.32
Untitled (Green Silver)	1949	58	78	412	566	7.10	7.26
AutumnRhythmN30	1950	267	526	795	1543	2.98	2.93
Mural on Indian Red Ground	1950	180	240	762	1018	4.23	4.24
Number 1 (Lavander mist)	1950	221	300	744	1021	3.37	3.40
Number 25	1950	25	96	249	966	9.96	10.06
Number 32	1950	269	458	607	1044	2.26	2.28
One: Number 31	1950	270	531	498	1000	1.84	1.88
Number 2	1951	104	79	800	586	7.69	7.42
Number 4	1951	77	64	569	465	7.39	7.27
Red, Yellow, Orange …	1951	60	90	656	998	10.93	11.09
Convergence	1952	237	390	789	1302	3.33	3.34
Number 11 (Blue Poles)	1952	212	489	579	1365	2.73	2.79
Paradigm R2	1952	91	165	1353	2488	14.87	15.08
Greyed rainbow	1953	183	244	630	843	3.44	3.45
Ocean greyness	1953	147	229	1027	1600	6.99	6.99
White light	1954	122	97	766	600	6.28	6.19

Images stored in JPG files were transformed into grayscale images with pixel value G. The classic conversion formula

$$G(k) = 0.299\mathrm{R(k)} + 0.587\mathrm{G(k)} + 0.114\mathrm{B(k)} \qquad (7)$$

was used, where k denotes a pixel, R, G, B represent the three bands (red, green, blue, respectively) stored in the files. The coefficients in (7) represent standards typically used to calculate luminance from RGB images (Rec.ITU-R BT.601-7). The grayscale images were then binned into n_b=10 categories. Such a number was found after some initial trials with increasing n_b, until geological entropy parameters were statistically stabilized , as shown in the

Supplementary Information (Figures S11-S19). Using n_b=10, the maximum entropy ($H_{\max}$) of the system can be computed analytically as $H_{\max}$=2.46.

Results

Analysis of two representative images

Two representative paintings were selected for detailed analysis to illustrate how geological entropy identifies and quantifies spatial order. These works represent distinct moments in Pollock's Action Painting period: *Composition with Pouring II* (Figure 2a), painted in 1943 at the beginning of the period; *Number 3 (1949): Tiger* (Figure 3a), painted in 1949, at the height of Pollock's mature drip technique.

Composition with Pouring II is often cited as one of Pollock's first drip paintings, although conservation analyses (pigments, binding media, cross-sections) showed that most of the work was executed using traditional brush techniques and artists' tube paints[32]. *Number 3 (1949): Tiger* was created entirely through the "all-over" method, when Pollock's drip method relied heavily on industrial materials such as enamel and alkyd paints, marking a clear departure from the more conventional methods still present in *Composition with Pouring II*. The canvas was placed on the floor, and Pollock used continuous, rhythmic pouring, flicking, and dripping with thinned commercial enamels. Traditional brushwork disappears, replaced by dense, interlocking paints that form a web-like surface typical of his 1949 output. The title "Tiger" was assigned later and has no representational basis. The all-over technique generates a distinctive spatial effect in which paint alternates between surface and depth without a central focal point, creating what critics such as Clement Greenberg described as "optical space".

Geological entropy metrics reflect the differences in technique and spatial organization in the two paintings. Figures 2b and 3b show the images after discretization into $N_b = 10$ classes (resulting in H_{max}=2.46) using isotropic and directional bandwidths of 50 pixels, with no resolution threshold. Figures 2c and 3c present the resulting entrograms and statistics. *Composition with Pouring II* exhibits lower H_{R0} and H_0 than *Number 3 (1949): Tiger*. Based on previous studies and the conceptual model in Figure 6, this indicates higher spatial order in the earlier painting. A lower $H_{R0} = 0.59$ in *Composition with Pouring II* suggests reduced categorical variability at short scales, implying fewer repeating patterns and greater structural coherence, compared to *Number 3 (1949): Tiger*, which has $H_{R0} = 0.67$.

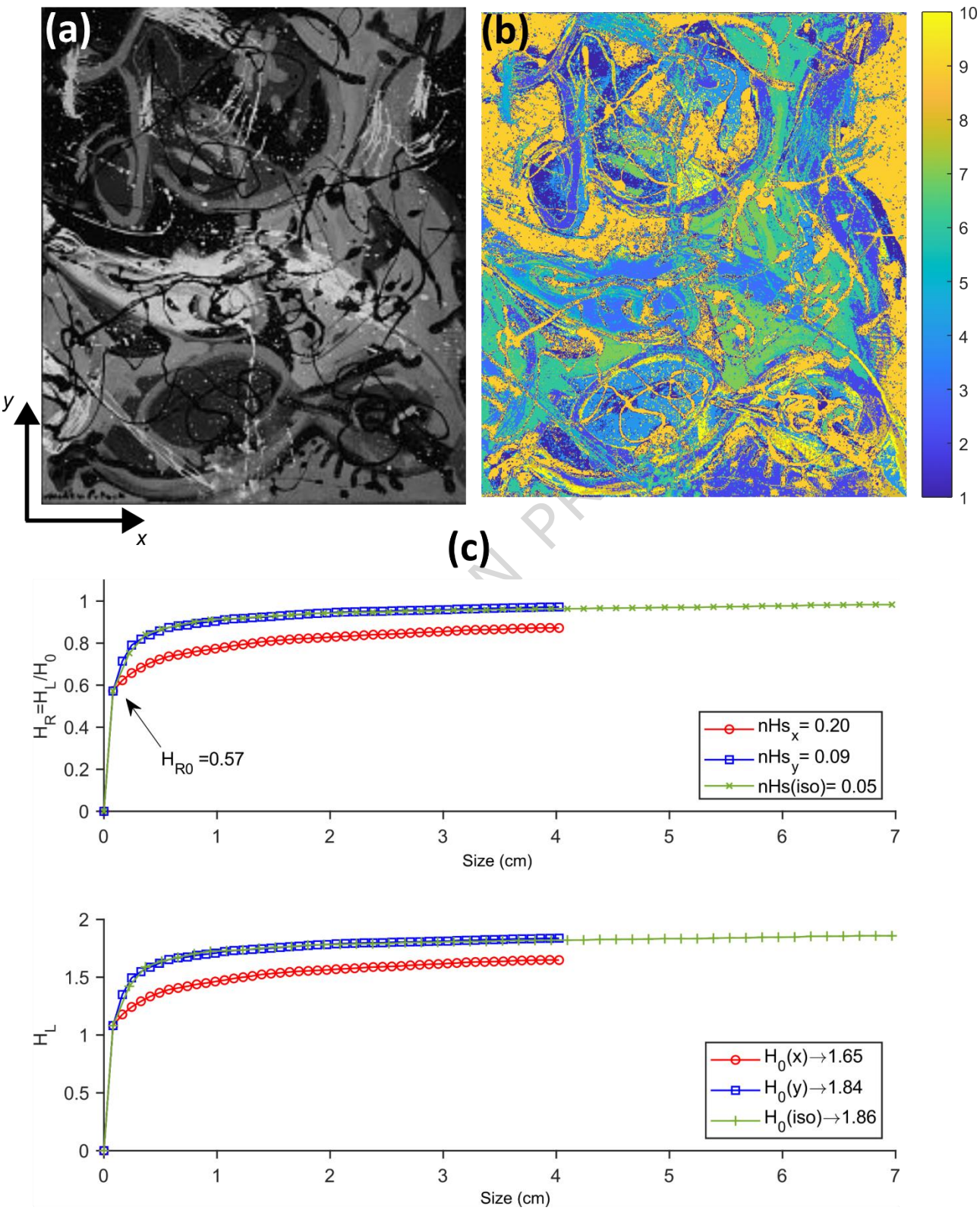
(a)
(b)
y
x
10
9
8
7
6
5
4
3
2
1
(c)
$H_R=H_L/H_0$
H_{R0} =0.57
nHs$_x$= 0.20
nHs$_y$= 0.09
nHs(iso)= 0.05
Size (cm)
H_L
H_0(x)→1.65
H_0(y)→1.84
H_0(iso)→1.86
Size (cm)

Figure 2

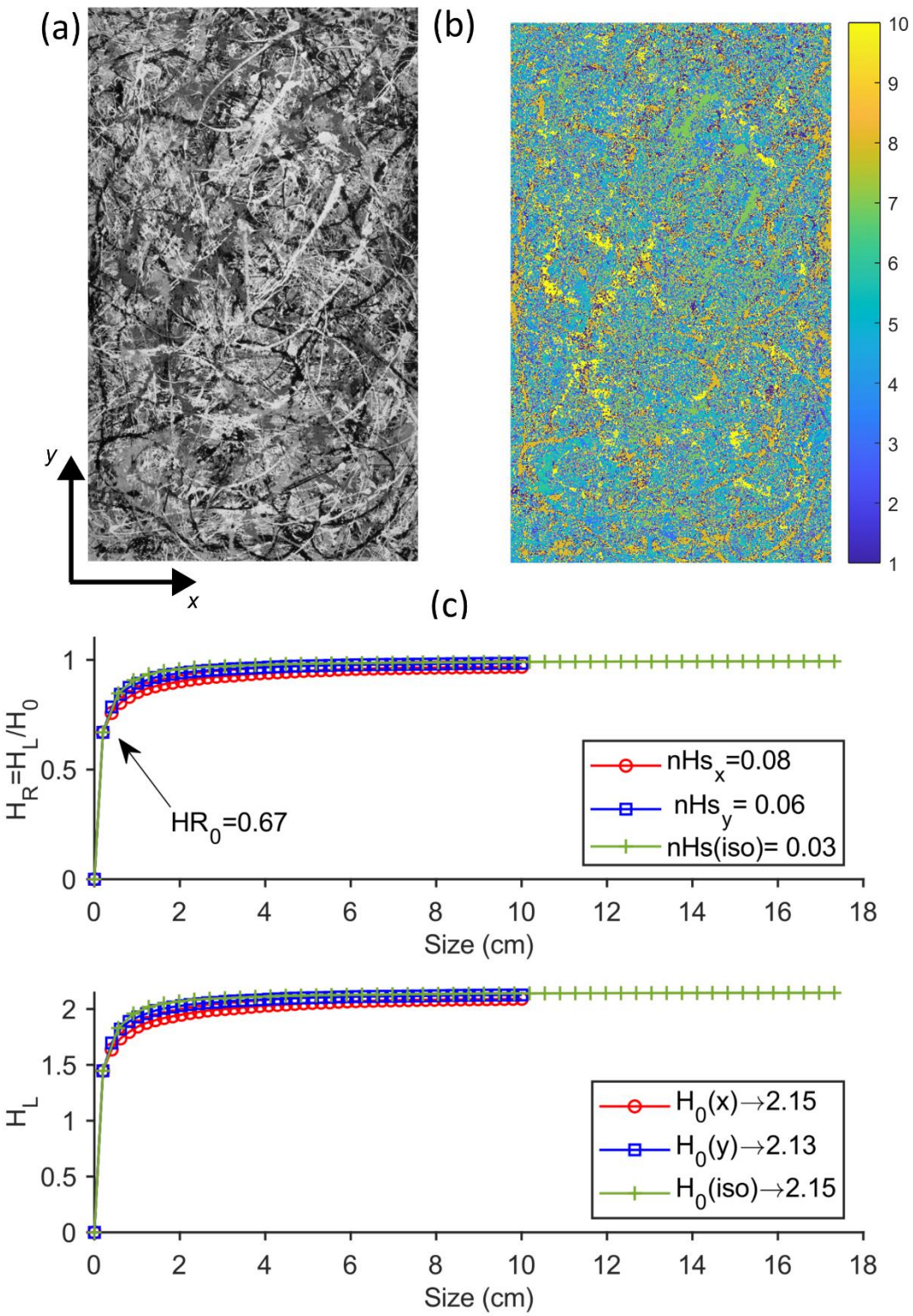
(a)
(b)
y
x
10
9
8
7
6
5
4
3
2
1
(c)
$H_R=H_L/H_0$
HR_0=0.67
nHs_x=0.08
nHs_y= 0.06
nHs(iso)= 0.03
Size (cm)
H_L
$H_0(x)\rightarrow 2.15$
$H_0(y)\rightarrow 2.13$
$H_0(iso)\rightarrow 2.15$
Size (cm)

Figure 3

Anisotropy in spatial order is also evident, especially in *Composition with Pouring II*. Here, the horizontal direction yields $nHs = 0.20$, while the vertical direction gives $nHs = 0.09$, producing an anisotropy ratio $\varepsilon = 2.22$. This indicates greater discontinuity horizontally, as the entrogram approaches maximum entropy more rapidly. Visually, this aligns with the pattern distribution in Figure 2b. By contrast, *Number 3 (1949): Tiger* shows much lower entropic scales and weaker anisotropy, as $nHs = 0.08$ horizontally and $nHs = 0.06$ vertically, giving $\varepsilon = 1.33$. These values are lower than in *Composition with Pouring II*, particularly for what concerns the horizontal direction. Moreover, H_{R0} and H_0 are consistently higher in all directions, revealing more disordered, quasi-isotropic patterns characteristic of Pollock's mature drip technique.

These findings align with Pollock's artistic evolution. In *Composition with Pouring II*, dripped elements are limited, and only the black paint layer uses a drip technique with commercial enamel. Art historians classify this work as transitional. Pollock was experimenting with new materials but had not yet embraced the fully "all-over" method of 1947–1950. Its three distinct, non-overlapping layers of color indicate deliberate, sequential application rather than spontaneous improvisation. Only the final dripped black layer, applied on a horizontal canvas, anticipates the looping poured lines that later defined his style.

Geological entropy metrics capture the change in anisotropy over time, which can be linked to Pollock's evolving mobility around the canvas. For *Composition with Pouring II*, Pollock employed more localized movements and occasional upright work. By contrast, in 1949 he adopted a full 360° approach, walking around and over the canvas, consistent with documented footage and contemporary accounts. This physical shift corresponds directly to the more

isotropic, highly disordered patterns observed in *Number 3 (1949): Tiger*. In this regard, the analysis of late-time paintings aligns well with previous studies focusing on anisotropy in Pollock's paintings using fractals[30].

Ensemble of images 1943-1954

The evaluation of the full set of images reveals a clear transition in the spatial order of Pollock's paintings, offering however a new perspective on the evolution of his technique in terms of anisotropy in the spatial order of painting patterns. Figure 4 presents the GEOENT results for all analyzed works. The left panels display the calculated relative entropy H_{R0}(top), the normalized isotropic entropic scale nHs(middle), and the global entropy H_0(bottom). Each metric is accompanied by a red continuous line connecting the median value (M_{HR0}, M_{nHs}, and M_{H0}) for paintings grouped by year of creation, and a dotted thin line connecting the mean values. The right panels summarize these values as boxplots for each year.

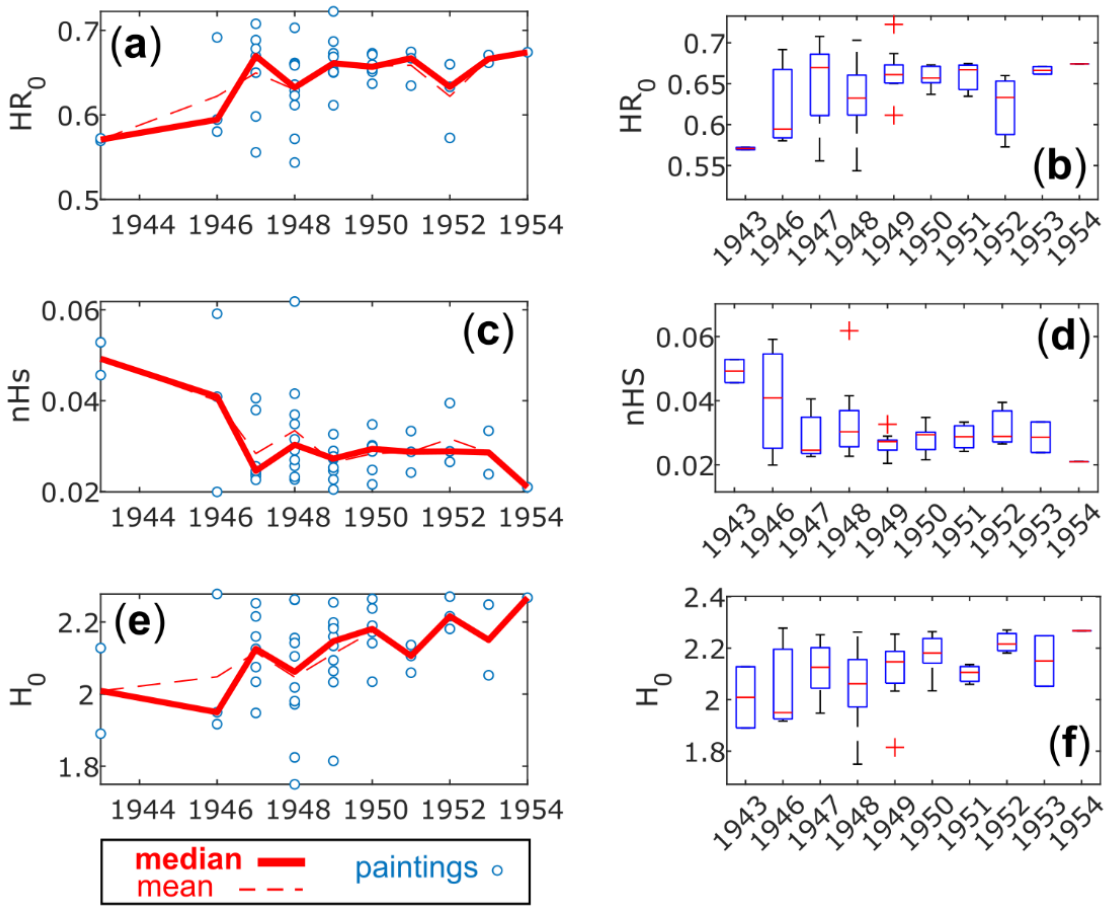

Figure 4

The temporal trends of M_{HR0} and M_{nHs} indicate two distinct phases in Pollock's artistic development. From 1943 to 1946, M_{HR0} increased from 0.57 to 0.67, while M_{nHs}decreased from 0.05 to 0.03. This pattern suggests a shift toward greater spatial disorder in the early Action Painting years. From 1947 to 1954, both indicators stabilize (approximately 0.64 and 0.03, respectively), implying that Pollock maintained a relatively consistent level of spatial disorder once his mature method was established.

Global entropy H_0 behaves differently from the other two indicators. Over the entire period from 1943 to 1954, M_{H0} gradually increases from 2.00 to 2.27, *i.e.* it tends to the maximum entropy for this number of categories ($H_{\max} = 2.46$ for $n_b = 10$). This trend is broadly consistent with a

progression from more to less ordered patterns at the scale of entire paintings. However, unlike $H_{R0}$and nHs, H_0 does not show the sharp transition between 1946 and 1947 and even exhibits a slight decrease from 1943 to 1946, contrasting with the behavior of the other indicators during these early years.

Directional entrograms (Figure 5) provide further insight. Normalized entropic scales were computed along the horizontal (nHs_x) and vertical (nHs_y) directions. Significant anisotropy in spatial order was identified across the corpus. In the early period, $nHs_x$is markedly higher than nHs_y. For instance, in 1943 the median horizontal value is 0.08, compared with 0.09 in the vertical direction, producing an anisotropy ratio $\varepsilon = 2.09$. Note that the vertical entropic scale is more similar to the isotropic value (0.05) than the horizontal entropic scale. According to the conceptual model in Figure 1, this evidence suggests that Pollock's drips in 1943 were shorter along the horizontal axis than along the vertical one.

Over time, the median values of nHs_x and nHs_y both decrease, although the horizontal component declines more rapidly. By 1954, nHs_x =0.07 and nHs_y=0.05. As a result, the anisotropy ratio steadily diminishes, reaching $\varepsilon = 1.38$ by 1954. This indicates that Pollock's drips became shorter and more similar in length across both directions as his technique matured, still maintaining preferential order along the vertical direction.

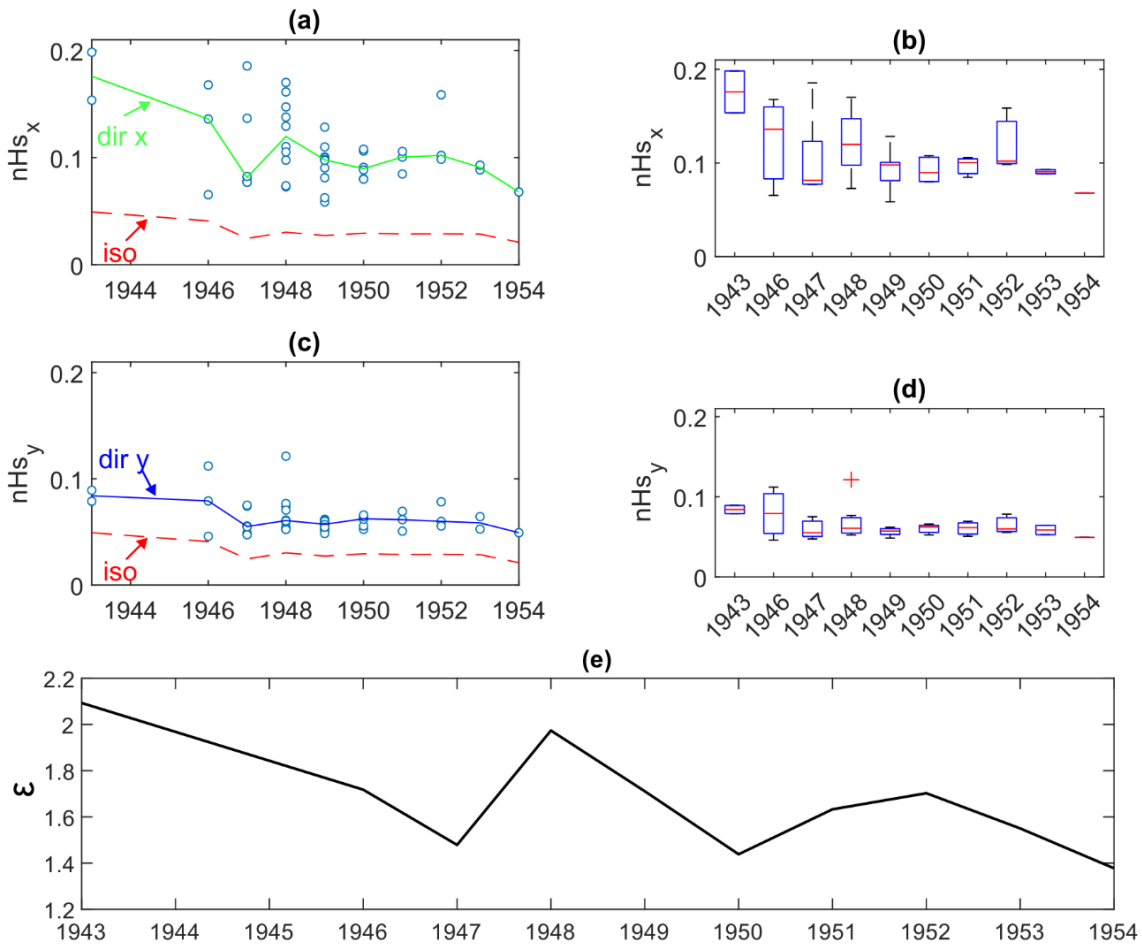

Figure 5

Comparison with fractal analyses

Geological entropy is derived from Shannon's information entropy, which has a well-established relationship with fractal analysis.[19] To contextualize our findings, we compared the geological entropy indicators obtained in this study with classic results from fractal analyses of Pollock's paintings[33], focusing in particular on the temporal evolution of fractal dimension *D* as reported by Taylor [31] (Figure 6). All geological entropy metrics showed strong agreement with the fractal dimensions reported by Taylor[31], supporting the conclusion that these metrics provide a

consistent alternative descriptor of Pollock's artistic evolution. However, there are key differences among the metrics worth highlighting and discussing.

The close correspondence between the temporal trends of fractal dimension D and the one-lag relative geological entropy H_{R0} is striking. Figure 6a compares D with the median relative geological entropy (M_{HR0}) computed for each year in our dataset. Taylor [31] found a notable change in the trend of D around 1947, which is highlighted in this plot by the use of the two background colors. In the "transition" phase, D shows a steeper increase than in the "drip" phase. Our results show a consistent behavior, qualitatively described by a gradient formed by an angle of π/3 in radians (or 60°) before 1947 and an angle of π/6 (or 30°) after 1947, i.e. the disorder increases at a rate half than that during the "transition" period.

A similar comparison was performed using the entropic scale nHs (Figure 6b-d), which also reflects spatial order. Because lower nHs corresponds to higher disorder and is inversely related to both HR_0 and D, we plotted nHs using a reverse vertical scale to facilitate comparison. Figure 5b to Figure 5d illustrate, respectively, the normalized entropic entropy using an isotropic bandwidth, using an anisotropic bandwidth along x and using an anisotropic bandwidth y.

It was found that rate at which the isotropic entrogram scale nHs increases is not ast steep in the transition period (Figure 6b) as obtained from HR_0. Specifically, nHs is better described of π/4 (or 45°) before 1947. By contrast, an angle of π/6 (or 30°) after 1947 describes more satisfactorily the data. A similar behavior was found along the horizontal direction (Figure 6c). The step is milder, and the overall trend from 1943 to 1954 seems described more by a linear increase in spatial disorder over time compared the two-phase trend observed for HR_0. Along the vertical direction (Figure 6d), the behavior closely mirrors both the results of HR_0 and the fractal

dimension *D*, with spatial disorder increasing more rapidly during the transition phase 1943-1947 (angle of π/3) and more gently thereafter (angle of π/6).

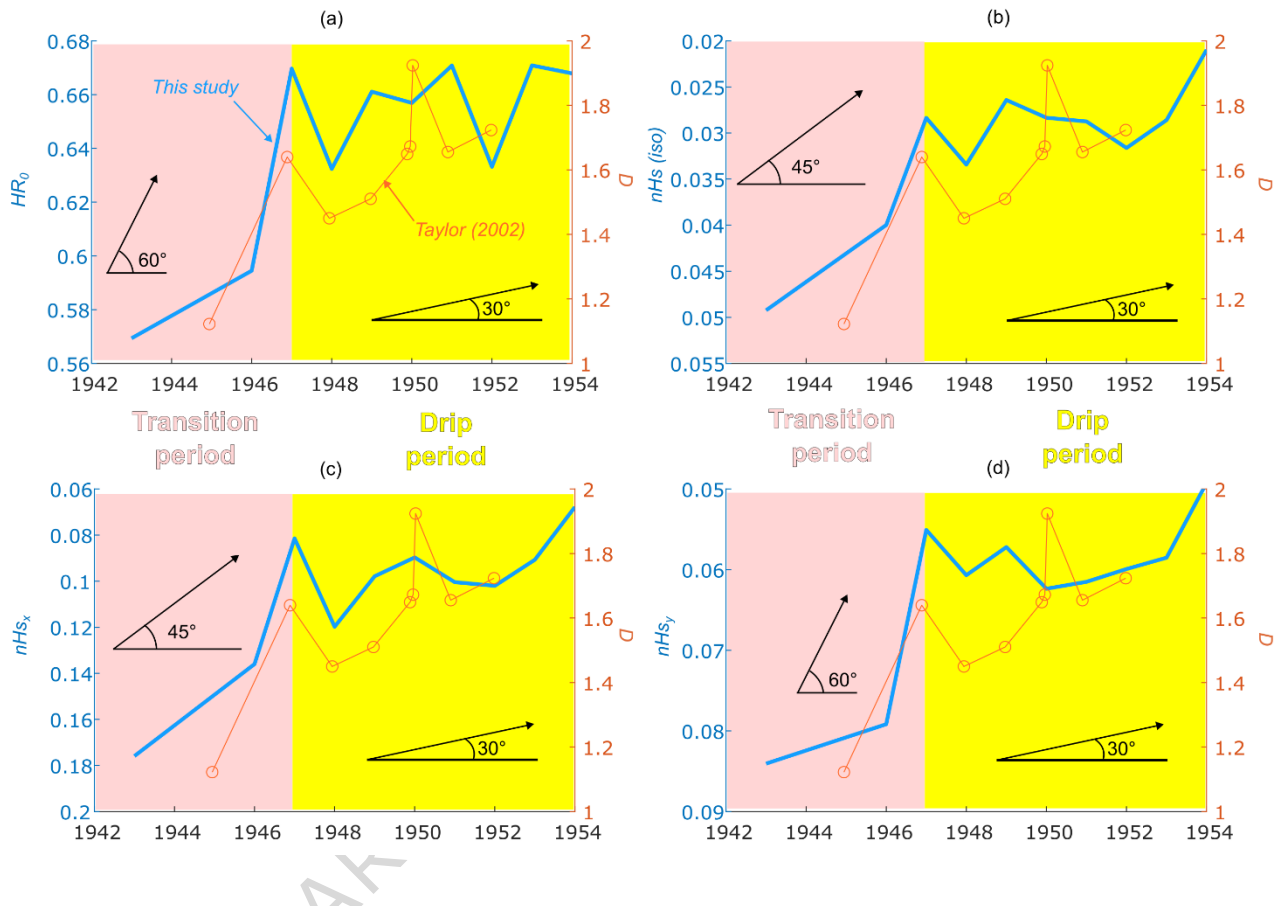

Figure 6

These findings suggest that Pollock may have systematically intensified spatial disorder along the horizontal direction more than along the vertical one throughout the period studied. One possible explanation is that, during his mature Action Painting period, Pollock increasingly favored large rectangular canvases, many of which were oriented horizontally and painted on the floor, a format that has been widely documented in art-historical studies and archival photographs. This format could have unintentionally encouraged Pollock to refine his dripping technique preferentially along the horizontal axis. Because his painting movements often followed Lévy-flight–like trajectories, the extended horizontal dimension may have allowed

greater variability in step size. Over time, Pollock may therefore have gradually reduced the effective step size along the horizontal direction while maintaining a more stable pattern along the vertical axis.

Discussion

This study showed that directional geological entropy (DGE) can be successfully applied to Jackson Pollock's Action Paintings created between 1943 and 1954. For the first time, geological entropy is shown to quantify spatial order in complex, seemingly chaotic patterns outside the geosciences, the field in which the method was originally developed. Pollock's paintings therefore provide an effective test case for the broader applicability of DGE to non-geological systems.

Regarding Pollock's work specifically, DGE produced results consistent with established fractal analyses. In particular, our analysis corroborates the widely accepted transition from an experimental phase (1943–1947), during which he developed the drip-and-pour technique, to a mature period (1947–1954) marked by more stable and highly disordered patterns. This agreement supports DGE as a robust alternative framework for evaluating order and disorder in Pollock's paintings. Given its success here, DGE may prove valuable for studying other artists whose works exhibit turbulent or chaotic structures. Moreover, unlike fractal analysis, DGE does not require statistical self-similarity across multiple orders of magnitude and can therefore be applied to size-limited artworks.

Beyond this consistency, DGE reveals a key feature not captured by previous approaches, namely the presence and temporal evolution of anisotropy in spatial order. . The results show

systematically higher disorder along the horizontal direction than along the vertical one, with the anisotropy ratio decreasing over time. This directional asymmetry provides new insight into Pollock's painting process. It may reflect the artist's increasing use of large rectangular canvases and changes in his movement patterns, including more refined Lévy-flight–like trajectories.

Overall, these findings demonstrate that DGE not only reproduces known characteristics of Pollock's work but also uncovers previously unrecognized directional structure. This suggests that entropy-based approaches offer a powerful and flexible framework for analyzing complex visual patterns. Future applications may extend to other artists or cultural artifacts exhibiting apparently chaotic structures, as well as to questions related to technique and authentication.

Author Contributions

Conceptualization: Daniele Pedretti. Data curation: Daniele Pedretti. Formal analysis: Daniele Pedretti. Funding acquisition: Daniele Pedretti. Investigation: Daniele Pedretti. Methodology: Daniele Pedretti. Project administration: Daniele Pedretti. Resources: Daniele Pedretti. Software: Daniele Pedretti. Supervision: Daniele Pedretti. Validation: Daniele Pedretti. Visualization: Daniele Pedretti

Acknowledgements

The work has been carried out in the frame of the "Progetti d'Eccellenza 2023–2027" MUR project granted to the Department of Earth Sciences "A. Desio" (no grant number).

Conflict of Interest

The author declares no competing financial or non-financial interests.

Data and code availability statement

The datasets generated during the current study and the underlying code for this study are available in GitHub and can be accessed via this link https://github.com/hydrogeolab/DGEPollock , with an example of a low-resolution image for the analysis of *Composition with pouring II.*

References

1. Taylor, R. P., Micolich, A. P. & Jonas, D. Fractal analysis of Pollock's drip paintings. *Nature* **399**, 422–422 (1999).
2. Taylor, R. P., Micolich, A. P. & Jonas, D. Fractal expressionism. *Phys. World* **12**, 25 (1999).
3. Mureika, J. R. Fractal dimensions in perceptual color space: A comparison study using Jackson Pollock's art. *Chaos: An Interdisciplinary Journal of Nonlinear Science* **15**, 043702 (2005).
4. Coddington, J., Elton, J., Rockmore, D. & Wang, Y. Multifractal analysis and authentication of Jackson Pollock paintings. in *Computer Image Analysis in the Study of Art* vol. 6810 131–142 (SPIE, 2008).

5. Halsall, F. Chaos, Fractals, and the Pedagogical Challenge of Jackson Pollock's 'All-Over' Paintings. *Journal of Aesthetic Education* **42**, 1–16 (2008).
6. Alvarez-Ramirez, J., Ibarra-Valdez, C. & Rodriguez, E. Fractal analysis of Jackson Pollock's painting evolution. *Chaos, Solitons & Fractals* **83**, 97–104 (2016).
7. Fairbanks, M. S. *et al.* A question of Jackson Pollock's balance: using lacunarity and fractal analysis to distinguish poured paintings by adults and children. *Front. Phys.* **13**, (2025).
8. Mureika, J. R., Dyer, C. C. & Cupchik, G. C. Multifractal structure in nonrepresentational art. *Phys. Rev. E* **72**, 046101 (2005).
9. Taylor, R. P. *et al.* Authenticating Pollock paintings using fractal geometry. *Pattern Recognition Letters* **28**, 695–702 (2007).
10. Martins, A. "NO CHAOS, DAMN IT!" Extracting paint maps from Macro-X-Ray Fluorescence scanning data to deconstruct Jackson Pollock's "action painting" in Number 1A, 1948. *www. ip4ai. ugent. be* 27 (2018).
11. Jones-Smith, K. & Mathur, H. Revisiting Pollock's drip paintings. *Nature* **444**, E9–E10 (2006).
12. Jones-Smith, K., Mathur, H. & Krauss, L. M. Drip Paintings and Fractal Analysis. *Phys. Rev. E* **79**, 046111 (2009).
13. Machado, J. T. & Lopes, A. M. Artistic painting: A fractional calculus perspective. *Applied Mathematical Modelling* **65**, 614–626 (2019).

14. Al-Ayyoub, M., Irfan, M. T. & Stork, D. G. Boosting multi-feature visual texture classifiers for the authentication of Jackson Pollock's drip paintings. in *Computer Vision and Image Analysis of Art II* vol. 7869 140–149 (SPIE, 2011).
15. Choi, J., Ju, L., Li, J. & Tu, Z. Information extraction and artwork pricing. Preprint at https://doi.org/10.48550/arXiv.2302.08167 (2023).
16. Pessa, A. A. & Ribeiro, H. V. ordpy: A Python package for data analysis with permutation entropy and ordinal network methods. *Chaos: An Interdisciplinary Journal of Nonlinear Science* **31**, (2021).
17. Shannon, C. E. A mathematical theory of communication. *Bell system technical journal* **27**, 379–423 (1948).
18. Zmeskal, O., Dzik, P. & Vesely, M. Entropy of fractal systems. *Computers & Mathematics with Applications* **66**, 135–146 (2013).
19. Chen, Y. Equivalent relation between normalized spatial entropy and fractal dimension. *Physica A: Statistical Mechanics and its Applications* **553**, 124627 (2020).
20. Mandelbrot, B. B. Is Nature Fractal? *Science* **279**, 783–783 (1998).
21. Bianchi, M. & Pedretti, D. Geological entropy and solute transport in heterogeneous porous media. *Water Resour. Res.* **53**, 4691–4708 (2017).
22. Bianchi, M. & Pedretti, D. An Entrogram-Based Approach to Describe Spatial Heterogeneity With Applications to Solute Transport in Porous Media. *Water Resources Research* **54**, 4432–4448 (2018).

23. Turcotte, D. L. Fractals in geology and geophysics. *PAGEOPH* **131**, 171–196 (1989).
24. Neuman, S. P. Universal scaling of hydraulic conductivities and dispersivities in geologic media. *Water Resour. Res.* **26**, 1749–1758 (1990).
25. Koltermann, C. E. & Gorelick, S. Heterogeneity in sedimentary deposits: A review of structure-imitating, process-imitating, and descriptive approaches. *Water Resources Research* **32**, 2617–2658 (1996).
26. Pedretti, D. Heterogeneity-controlled uncertain optimization of pump-and-treat systems explained through geological entropy. *Int J Geomath* **11**, 22 (2020).
27. Ye, Z. *et al.* Evaluation of Connectivity Characteristics on the Permeability of Two-Dimensional Fracture Networks Using Geological Entropy. *Water Resources Research* **57**, e2020WR029289 (2021).
28. Zhou, C., Ye, Z., Yao, C., Fan, X. & Xiong, F. Estimation of the anisotropy of hydraulic conductivity through 3D fracture networks using the directional geological entropy. *International Journal of Mining Science and Technology* https://doi.org/10.1016/j.ijmst.2024.01.004 (2024) doi:10.1016/j.ijmst.2024.01.004.
29. Pedretti, D. & Bianchi, M. GEOENT: A Toolbox for Calculating Directional Geological Entropy. *Geosciences* **12**, 206 (2022).
30. Alvarez-Ramirez, J., Ibarra-Valdez, C., Rodriguez, E. & Dagdug, L. 1/f<math><mn is="true">1</mn><mo is="true">/</mo><mi

is="true">f</mi></math>-Noise structures in Pollocks's drip paintings. *Physica A: Statistical Mechanics and its Applications* **387**, 281–295 (2008).

31. Taylor, R. P. Order in Pollock's chaos. *Scientific American* **287**, 116–121 (2002).

32. Rosi, F. *et al.* Jackson Pollock's Drip Paintings: Tracing the Introduction of Alkyds Through Non-invasive Analysis of Mid-1940s Paintings. https://doi.org/10.1039/9781788016384-00001 (2020) doi:10.1039/9781788016384-00001.

33. Mureika, J. R., Cupchik, G. C. & Dyer, C. C. Multifractal Fingerprints in the Visual Arts. *Leonardo* **37**, 53–56 (2004).

Figure captions

Figure 1. Conceptual behavior of directional entrograms. The image in panel (a) has an isotopic disorder, as observed by the similar scaling of the entrograms in the two direction (dir1 is parallel to the horizontal axis x; dir2 is parallel to the vertical axis y). By contrast, the image in panel (b) has an anisotropic disorder, with the horizontal direction being more persisten than the vertical direction. Panels (c) and (d) show the entrograms respectively of (a) and (b). The impact of anisotropy and the preferential disorder in one direction is striking in (d), which is also the one with lower H_{R0}. The entropic scale nHs is higher along the direction with higher disorder.

Figure 2(a) Analysis of "*Composition with pouring II" (1943)*. (a) The image in its original colors, derived from images available at WikiArt (https://www.wikiart.org/), cropped and reprocessed ; (b) the image discretized in n_b=10 categories; (c) the resulting normalized (top) and not-normalized (bottom) directional entrograms and corresponding metrics.

Figure 3 Analysis of "*Number 3(1949): Tiger*" (1949). (a) The image in its original colors, derived from images available at WikiArt (https://www.wikiart.org/), cropped and reprocessed; (b) the image discretized in n_b=10 categories; (c) the resulting normalized (top) and not-normalized (bottom) directional entrograms and corresponding metrics.

Figure 4 Evolution over time of geological entropic indicators used to analyze the spatial order of Pollock's paintings. (a,b) local geological entropy (HR_0); (c,d) normalized entropic scale (nH_S); (e,f) global entropy (H_0). In the left boxes, median and mean are overlapped to the calculated values of the

individual paintings, by year of creation. In the right boxes, boxplots of the invidual paintings by year of creation are reported.

Figure 5 Analysis of the ensemble of images. (a) Evolution of the median normalized entropic scale along the horizontal direction x (nHs_x) and (b) boxplots of the full distribution by year; (c) Evolution of the median normalized entropic scale along the vertical direction x (nHs_y) and (d) boxplots of the full distribution by year. (e) Evolution of the anisotropy ε, calculated as the ratio between the median values nHs_x and nHs_y.

Figure 6 Comparison between the geological entropy metrics found in this study and the fractal dimension D reported by Taylor 31.